IEEE Photonics Journal
An IEEE Photonics Society Publication

Open Access

Strategies for Upgrading an Operator's Backbone Network Beyond the C-Band: Towards Multi-Band Optical Networks

Volume 13, Number 2, April 2021

Dimitris Uzunidis
Evangelos Kosmatos
Chris Matrakidis
Alexandros Stavdas
Andrew Lord

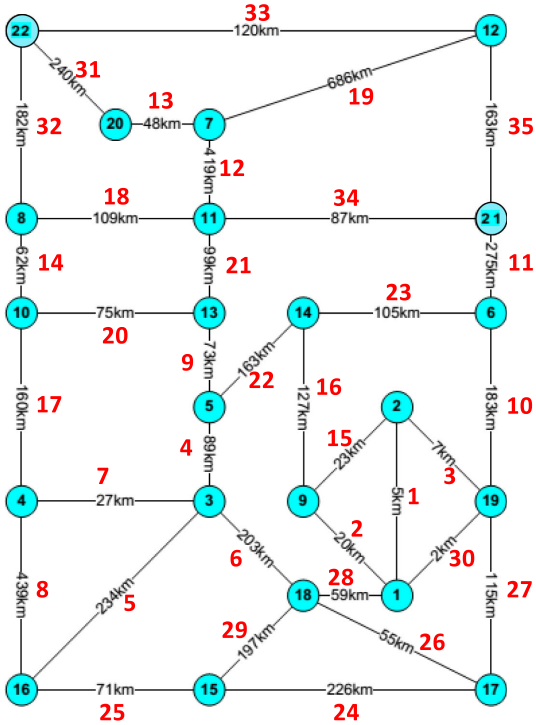

DOI: 10.1109/JPHOT.2021.3054849

Strategies for Upgrading an Operator's Backbone Network Beyond the C-Band: Towards Multi-Band Optical Networks

Dimitris Uzunidis,[1] **Evangelos Kosmatos**,[1] **Chris Matrakidis**,[1] **Alexandros Stavdas**,[2] **and Andrew Lord**[3]

[1]OpenLightComm Ltd, The Ross Building, Adastral Park, IPSWICH IP5 3RE, U.K.
[2]Department of Informatics and Telecommunications, University of Peloponnese, Tripolis 22100, Greece
[3]Research and Innovation, BT, Ipswich IP5 3RE, U.K.

DOI:10.1109/JPHOT.2021.3054849

Manuscript received December 3, 2020; revised January 19, 2021; accepted January 21, 2021. Date of publication January 26, 2021; date of current version March 3, 2021. This work was supported by the H2020 METRO-HAUL Project, EU Grant Agreement 761727. Corresponding author: Dimitris Uzunidis (e-mail: duzunidis@hotmail.com).

Abstract: Telecommunication networks are becoming the central linking institution of the Fourth Industrial Revolution. To cope with the associated capacity and connectivity challenges, transportation networks may explore the -neglected so far- remaining transmission bands in the second and third low attenuation windows of the optical fibre overcoming the C-band barrier. To assess the potential of optical multi-band transmission systems to upgrade a European Operator's network, we have developed a planning tool based on a routing engine that exploits a novel Physical Layer Aware, Routing, Modulation and Spectral Assignment algorithm. We considered unrepeatered transmission exploiting fibre amplifiers tailored to each transmission band. Taking into account the performance of close to commercialization fibre amplifier devices, we estimated the impact for the most detrimental effects in multi-band transmission like ASE accumulation, FWM and SRS. With the aid of this planning tool, we demonstrate the potential of multi-band systems to upgrade network capacity without compromising the connectivity between Core nodes, albeit new physical layer challenges. Nevertheless, it is shown that multi-band systems allow higher operational flexibility that may slow-down the need to deploy additional C-band fibres. Moreover, we have shown that the roll out of these multi-band systems could be planned in phases in order to limit first-day capital expenditure.

Index Terms: Optical Multi-Band Systems, Physical Layer Impairments, Routing Modulation and Spectral Assignment algorithms, Elastic Optical Networks.

1. Introduction

The proliferation of Fourth Industrial Revolution applications associated with Internet of Things and other Machine-to-Machine communication systems and the advances in fixed and wireless access technologies to support them, will put, in turn, optical transport networks under a significant strain. In particular, as end-user bandwidth is surging and the aggregated traffic is funneled back into backbone networks, fresh solutions are inevitably required in this part of the network to overcome the upcoming capacity crunch and system gridlock. Moreover, as a result of the fusion of DataCentres and connectivity networks into clouds and the distribution of DataCentres in the

network periphery, an upscale in connectivity requirements between nodes in Core and Metro network segments is witnessed.

The emergence of "Elastic" Optical Networks (EONs) proved to be a landmark in the quest to maximise the utilisation of the available spectrum in the C-band and paved the way to achieve transportation rates beyond 100G, towards single wavelength 1 Tb/s line-rates. However, these advances are accompanied by a number of pitfalls. In particular, the primary objective of EONs is to increase the capacity of a point-to-point connection while maximising spectrum utilisation. Under EON, there are two alternative methods to upscale a line-rate to 200G/400G or 800G rates: a) either to operate at a higher baud-rate i.e. to consume extra optical bandwidth (a higher number of spectral slots); or b) to employ a higher modulation format. In the former case, (a), operation at higher-rates is made at the expense of the spectral slots left to provide inter-node connectivity which means that node connectivity is traded for higher capacity per channel. In turn, the inevitable exhaustion of the C-band will require Operators to "light-up" a higher number of fibres than they do today. Under the second alternative, (b), despite the remarkable advances in the attainable quality of transmission (QoT) performance -thanks to progress in digital signal processing (DSP)- higher single channel rates are achieved at the expense of lower reach. This again restricts inter-node connectivity. Furthermore, the deployment of high-capacity single-wavelength 400G/800G connections makes sense cost-wise only with highly-aggregated flows. This becomes increasingly difficult with the emergence of dramatically more dynamic traffic patterns [1].

The exploitation of the ultimate bandwidth potential of single mode fibre (SMF) in conjunction with EON-compatible transmission systems is providing a tangible solution to these challenges. Optical Multi-Band (*OMB*, hereafter) transportation systems [2]–[4] and a complementary multiplexing technology that allow the exploitation of the second and third low attenuation windows of SMF [5], [6], fully utilize the potential of WDM/Wavelength Routed Networks (WRNs) and EONs. Recently, a number of studies were published probing to OMB deployment challenges using experimental [7], [8] or analytical methods [9]–[11].

In this work, we present and evaluate strategies that employ OMB systems which may increase the transported capacity without compromising node connectivity in a national Operator's Core and Metro network. Moreover, we show the higher operational flexibility offered by more relaxed transportation schemes that exploit a coarser channel spacing. Under the latter scheme the channels are sparsely populated, meaning that the optical bandwidth is not treated as a scarce commodity as EON C-band-only systems do (these systems are designated as *legacy*, hereafter). Nevertheless, as the deployment of OMB systems has its own challenges, we are also trying to shed light on the pros and cons of multi-band transportation.

In particular, in Section 2 we present the overall objectives of this work and the approach which we have adopted to address the challenges. We elaborate the OMB amplifier connectivity mode and we present the formalism that accounts for the impact of physical layer effects on transmission performance. In Section 3, we elaborate the details of a routing engine for OMB networks. In Section 4, we detail the configuration and parameters of the systems under investigation as well as the optimization methods we have adopted for the operation of these systems. In Section 5, we use the routing engine of Section 3 to benchmark alternative configurations in terms of performance and scalability. Finally, we propose a roadmap for the introduction of OMB systems in a national network.

2. Methodology and Approach

The scope of this work is to assess the potential of OMB transmission systems to upgrade British Telecom (BT)'s "21st Century Network" (21CN) and to propose strategies for their introduction into this network. The network topology under study is schematically depicted in Fig. 1.

Currently, BT's 21CN network is employing C-band transmission systems in transparent connections. However, the exploitation of the L-band as well as the -so far neglected- other transmission bands like O, E, and S, is becoming increasingly plausible thanks to a wide range of advances in optoelectronic systems and sub-system associated to transceivers and optical amplifiers tailored

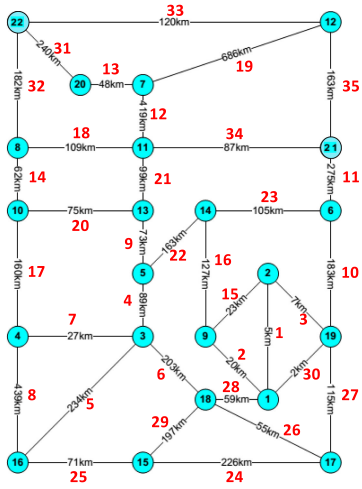

Fig. 1. Overview of BT's 21CN 22 node network with inter-node distances and link numbers.

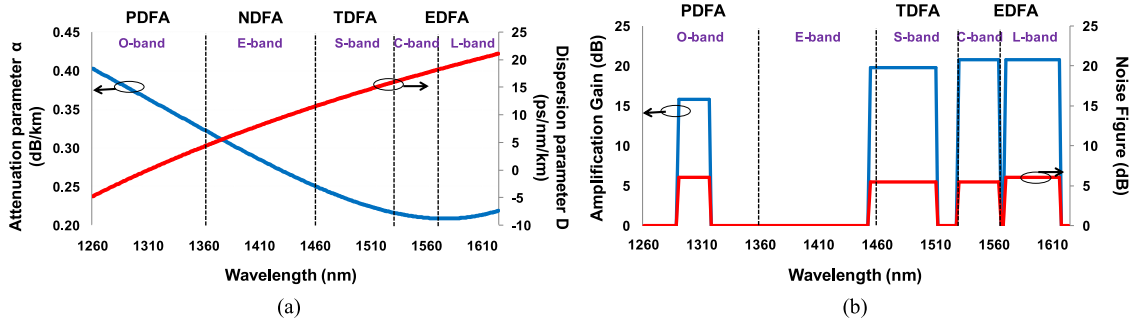

Fig. 2. (a) Attenuation and dispersion for the G.652D fibre in 1260 nm–1610 nm. (b) Performance of close to commercialization DFAs in the corresponding bands; a total input power of 0 dBm is assumed in all cases.

for these bands. To assess the potential of OMB transmission systems to increase the transported capacity -without compromising the attainable connectivity- in BT's 21CN network, we have developed a planning tool that employs a routing engine exploiting a novel Physical Layer Aware Routing, Modulation and Spectral Assignment algorithm (PLA-RMSA). For this reason, the remaining part of this and the next Sections are dedicated to elaborate the approach we have adopted to construct this PLA-RMSA engine.

2.1 Doped Fibre Amplifiers

The role of optical amplification is key for the scalability of an unrepeated network like the BT's 21CN. A number of amplification technologies for OMB systems exploiting Semiconductor Optical Amplifiers (SOAs) [12], Raman [13] or Doped Fibre Amplifiers have been proposed. In this work we are only considering the latter technology only, since the xDFA family demonstrates similar operational and performance features to C-band EDFAs making them very attractive for OMB transmission.

Fig. 2(a) shows the xDFAs which are tailored for the second and third low-attenuation window transmission bands (following the ITU standardisation nomenclature) together with the corresponding attenuation and second order dispersion values. As an example, praseodymium-DFA (PDFA) and thulium-DFA (TDFA) are employed for the O-band and the S-band, respectively, while a neodymium-doped fibre amplifier (NDFA) has been proposed for the E-band [14]. These DFA deployments feature sufficiently flat gain performance over a substantial spectral range, along with

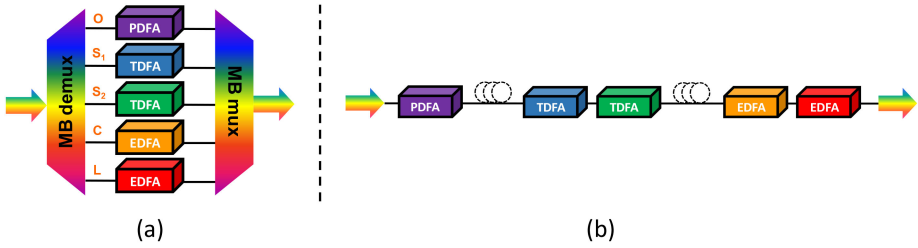

Fig. 3. Amplifier connectivity schemes: (a) parallel and (b) serial.

relatively low noise figures, ensuring high Quality-of-Transmission (QoT). In this respect, Fig. 2(b) depicts the typical systems-related performance for those DFAs with respect to gain, gain-flatness and noise figure at 0 dBm input power [15].

2.2 Two Configurations for the Positioning of DFAs

Unlike legacy, C-band only, systems which they use EDFAs only, in OMB systems the optical amplifiers are arranged in two possible layouts: the *parallel* and the *serial* as it is schematically illustrated in Fig. 3.

In the parallel configuration of Fig. 3(a), band- multiplexers/demultiplexers (mux/demux) are used to separate the amplification bands. In this scheme, the DFAs used in the different bands are collocated. As the band mux/demux devices have to be placed in tandem at every amplification stage, the loss figure of the already deployed C-band systems has to be re-iterated while the legacy EDFAs may have to be re-regulated to compensate for the extra loss. Therefore, the optical signal to noise ratio (OSNR) performance of existing systems could be somewhat degraded which means that system designs that incorporate operational (power) margins are necessary. This is introduced and detailed in Section 4 and 5. On the other hand, the advantage of this scheme is that the bands are totally decoupled, allowing an operator to make the most from the existing ducts for EDFAs: the optical amplifiers for the new transmission bands are housed in these ducts, preserving the huge investment made on the existing transportation infrastructure.

In the alternative arrangement, the optical amplifiers are placed in a cascade (serially) as in Fig. 3(b). This is appealing as it somewhat relaxes the previous OSNR degradation of the C-band links as no band filters are necessary to separate the bands and as such, no additional gain is needed to compensate their loss. Moreover, it allows to tailor the span between amplification stages for each band individually, depending on the actual amplifier performance. On the other hand, the main question for this configuration is the impact of the Gain Flattening Filters (GFF) of each DFAs, to the loss budget of other bands. This topic requires further investigation as in prior art [16]–[20], no more than two bands (C and L or S and C bands) were cascaded. Nevertheless, the configuration of Fig. 3(b) may require new amplifier ducts, at different locations from those currently employed for legacy EDFAs something that could significantly increase the deployment costs. Finally, a drawback of the serial configuration is that the channels that correspond to the optical pumping wavelengths for the different doped-fibre amplifiers of Fig. 3 have to remain unused for data transportation. Based on the above considerations, this study exploits only the parallel configuration.

2.3 Physical Layer Effects That Degrade an OMB System

The impact of transmission impairments on signal quality strongly depends on the local values of fibre attenuation and dispersion as well as the noise figure of the DFA employed in each band. However, as the main scope of this work is to incorporate physical layer modeling methods into an RMSA algorithm, we pursue a mathematical formalism that trades complexity with realistic RMSA simulation time. In particular, as numerical solutions incur a heavy computational burden that may prevent the routing engine from a timely response, we only consider closed-form

expressions, for the most detrimental transmission effects like Amplified Spontaneous Emission (ASE) accumulation, Four-Wave-Mixing (FWM) and Stimulated Raman Scattering (SRS). The impact of FWM is predominantly an intra-band phenomenon while its strength is different in different bands due to the different attenuation and second order dispersion values. On the other hand, the SRS is a phenomenon that couples bands together via a power exchange. The impact of these effects on a point-to-point (multi segment) fibre connection is assessed by means of the Optical Signal-to-Noise plus Interference Ratio (OSNIR) which is defined as

$$OSNIR = \frac{P_{ch} \cdot G_{SRS,i}}{P_{ASE} + P_{FWM}} \tag{1}$$

In (1) P_{ch} is the power per channel, P_{FWM} is the power of FWM interference and P_{ASE} is given by

$$P_{ASE} = \sum_{l=1}^{N_l} \left[\sum_{i=1}^{N_{s,l}} \left[hf\left(NF_i(\lambda) \cdot G_i(\lambda) - 1\right) B_0 \prod_{r=i+1}^{N_{s,l}} G_{SRS,r} \right] \Big/ \left(\prod_{m=1}^{N_{s,l}} G_{SRS,m} \right) \right]$$

where $G_i(\lambda)$ and $NF_i(\lambda)$ are wavelength dependent, representing the amplifier's gain and noise figure, respectively, at the i^{th} amplification stage. In the expression for the P_{ASE}, N_l denotes the number of links in an end-to-end path, $N_{s,l}$ denotes the number of fibre spans a link consists of; B_0 is the reference bandwidth equal to the width of three spectral slots (37.5 GHz).

To estimate the impact of FWM, the EGN model [21] is widely used as it is an accurate and reliable method. However, this model requires a considerable amount of numerical evaluations that make it unsuitable for inclusion in real-time, elaborate, optimization processes which is the objective of this work. The variant of EGN model [22] overcomes this limitation, but leads to erroneous estimations when the span length is smaller than 35 km. Moreover, it calculates P_{FWM} only for the central channel in a WDM comb while it does not account for unequal channel powers and/or for channels of dissimilar optical bandwidth and modulation formats. Since BT's 21CN network has span lengths shorter than 35 km while we need to estimate the physical layer performance for all channels in a link (and not only the central one), the model of [22] is of limited interest in our case. In contrast, our previous work in [23] overcomes these limitations while it is applicable to all transmission bands so it used here to estimate the impact of FWM; therefore, the P_{FWM} is given by

$$\begin{aligned} P_{FWM,slot} = {} & \frac{32}{27} \frac{\gamma^2 {L_{eff}}^2 P_0 {N_s}^2 c}{\lambda^2 B^2 D(\lambda) \sqrt{z_1}} \left(1 + \frac{4e^{-a(\lambda)L}}{\left(1 - e^{-a(\lambda)L}\right)^2}\right) \left({P_0}^2 asinh\left(\frac{\pi \lambda^2 D(\lambda) B^2}{8c} \sqrt{z_2}\right) \right. \\ & \left. + \sum_{n=-\frac{N_{slot}-1}{2}, n\neq 0}^{\frac{N_{slot}-1}{2}} {P_n}^2 \left(1 - \frac{5}{6}\Phi_n\right) \left| Log\left(\frac{n+1/2}{n-1/2}\right) \right| \right) \\ & - \frac{32}{27} \frac{\gamma^2 {L_{eff}}^2 P_0 {N_s}^2 c}{\lambda^2 B^2 D(\lambda) \sqrt{z_1 + 12L^2}} \frac{4e^{-a(\lambda)L}}{\left(1 - e^{-a(\lambda)L}\right)^2} \left({P_0}^2 asinh\left(\frac{\pi \lambda^2 D(\lambda) B^2}{8c} \sqrt{z_2 + 12L^2}\right) \right. \\ & \left. + \sum_{n=-\frac{N_{slot}-1}{2}, n\neq 0}^{\frac{N_{slot}-1}{2}} {P_n}^2 \left(1 - \frac{5}{6}\Phi_n\right) \left| Log\left(\frac{n+1/2}{n-1/2}\right) \right| \right) \end{aligned} \tag{2}$$

where $z_1 = (\frac{2}{a(\lambda)})^2 + 2L^2({N_s}^2 - 1)/(\sum_{k=x_1}^{x_2} \frac{1}{1+(2k\pi/(a(\lambda)L))^2})^2$, $z_2 = (\frac{2}{a(\lambda)})^2 + 2L^2({N_s}^2 - 1)$, $x_1 = -\frac{\lambda^2 B^2 D(\lambda) L {N_{slot}}^2}{16c}$, $x_2 = \frac{\lambda^2 B^2 D(\lambda) L {N_{slot}}^2}{2c}$ with N_{slot} to denote the total number of spectral slots. It is pointed out that the parameters fiber attenuation and local dispersion in Eq. (2) are wavelength dependent.

The index n accounts for the optical slots that, under EON, are consumed to transport channels within a given band, so $-(N_{slot} - 1)/2 \leq n \leq (N_{slot} - 1)/2$. P_n and P_0 denote the power for the n^{th}

interfering and the subject slot upon which the strength of FWM is measured, respectively; B is the (spectral) slot width, γ the nonlinear fibre coefficient, L the span length and N_s the number of fibre spans. The parameter Φ_n depends on modulation format of the nth channel and it takes the value of 1 for QPSK and 17/25 for 16-QAM [22]. Nevertheless, Eq. (2) is not applicable within a spectral range of $\sim$2 nm around the zero-dispersion wavelength.

To account for all types of FWM, Eq. (2) is decoupled into two parts: intra-slot and inter-slot FWM, given by Eq. (3) and (4) respectively. Intra-slot FWM refers to the degradation due to the interactions between the frequencies within the particular spectral slot only. On the other hand, inter-slot FWM estimates the strength of the effect due to the interaction of the particular spectral slot with all other n slots in the band. Based on these, Eq. (2) is modified as

$$P_{FWM,\text{intra}} = \frac{32}{27}\frac{\gamma^2 {L_{eff}}^2 {P_0}^3 {N_s}^2 c}{\lambda^2 B^2 D(\lambda)\sqrt{z_1}}\left(1+\frac{4e^{-a(\lambda)L}}{\left(1-e^{-a(\lambda)L}\right)^2}\right) asinh\left(\frac{\pi\lambda^2 D(\lambda) B^2}{8c}\sqrt{z_2}\right) - \frac{32}{27}\frac{\gamma^2 {L_{eff}}^2 {P_0}^3 {N_s}^2 c}{\lambda^2 B^2 D(\lambda)\sqrt{z_1+12L^2}}\frac{4e^{-a(\lambda)L}}{\left(1-e^{-a(\lambda)L}\right)^2} asinh\left(\frac{\pi\lambda^2 D(\lambda) B^2}{8c}\sqrt{z_2+12L^2}\right) \quad (3)$$

$$P_{FWM,\text{inter}} = \sum_{n=-\frac{N_{slot}-1}{2},n\neq 0}^{\frac{N_{slot}-1}{2}} {P_n}^2\left(1-\frac{5}{6}\Phi_n\right)\left|Log\left(\frac{n+1/2}{n-1/2}\right)\right|\frac{32}{27}\frac{\gamma^2 {L_{eff}}^2 P_0 {N_s}^2 c}{\lambda^2 B^2 D(\lambda)} \times\left(\frac{1}{\sqrt{z_1}}\left(1+\frac{4e^{-a(\lambda)L}}{\left(1-e^{-a(\lambda)L}\right)^2}\right)-\frac{1}{\sqrt{z_1+12L^2}}\frac{4e^{-a(\lambda)L}}{\left(1-e^{-a(\lambda)L}\right)^2}\right) \quad (4)$$

Finally, the SRS limits the performance of multi-band systems due to power transfer from the lower-wavelengths towards the higher-wavelengths found within the SRS gain bandwidth. Although the effect that leads to unequal channel power levels due to SRS can be partially mitigated by means of VOAs in transparent transit nodes, the OSNR degradation is still an issue for the lower wavelength channels due to power depletion. To calculate these gain/loss effects due to SRS for the j^{th} wavelength in the i^{th} fibre span, the following expression was used [24], [25]:

$$G_{SRS,i} = P_{tot,SRS}\frac{e^{\frac{g'\cdot B\cdot L_{eff}}{2A_e}(j-1)P_{tot,SRS}}}{\sum_m\left[P_{m,0}e^{\frac{g'\cdot B\cdot L_{eff}}{2A_e}(m-1)P_{tot,SRS}}\right]} \quad (5)$$

where g' is the Raman gain slope equal to $4.9\cdot10^{-27}$ m/(W$\cdot$Hz), A_e the effective cross sectional area of the fibre equal to 80 μm^2 and $P_{m,0}$ is the power of the m^{th} interfering channel at fibre input. The term $P_{tot,SRS}=\sum_m P_{m,0}$ is the sum of the power from all channels that interact within the SRS gain bandwidth. For the derivation of Eq. (5) an implicit use of the so-called *triangular approximation* for the Raman gain under which only the channels within a 15 THz range interact [26]. This means that the Raman gain outside this bandwidth is close to zero and can be ignored. The validity of this assumption has been verified via experimental [26] and numerical results [27], [28] showing to be in very good agreement (less than 1 dB in most cases). Therefore after Eq. (1) and (5), the channels under the SRS gain bandwidth do interact and they are simultaneously amplified/attenuated based on their relative position in this band.

In our analysis, secondary effects, like the impact of SRS on FWM, are not considered in a rigorous manner as a closed-form algebraic expression for this effect is not readily available. In particular, although the impact of SRS on FWM is studied in [7], [9]–[11], the formalism in [7] is not in a closed-form, which is problematic for its introduction into our PLA-RMSA algorithm, whilst in [9]–[11] ideal flattening filters are assumed after each fiber span. This is a rather restrictive condition which does not necessarily apply to the network under investigation here, as here the SRS Gain/Loss compensation is performed via a Wavelength Selective Switch (WSS) at the ingress of link and not per span as in [9]–[11]. In any case, one can observe from Fig. 4(b) of [9] that the impact of SRS on FWM is becoming significant for total launch powers greater than +21 dBm. The

TABLE 1
Variables and Parameters Used in the MB-RMSA Algorithm

Variable	*Description*	*Variable*	*Description*
G	network topology graph	d_s	source of demand d
N	set of network nodes	d_n	destination of demand d
E	set of bidirectional optical fibre links (edges)	d_t	duration of demand d
A	Set of amplifiers in the network	d_{lr}	Requested line-rate for demand d
B	set of active optical bands	k	number of shortest paths used in Yen's algorithm
C_B	set of available frequency slot units - FSUs for each optical band in the set B	K	set of k-shortest paths calculated using Yen's algorithm
T	Input traffic matrix	p_c	candidate path assigned to demand d
D	set of demands in increasing time of arrival order	r_c	candidate transmitter type assigned to demand d
D_t	average time duration of the demands	f_c	candidate set of FSUs assigned to demand d
D_i	average inter-arrival time between two consecutive demands	p_a	final path assigned to demand d
LR	set of available line-rates	r_a	final transmitter type assigned to demand d
R_B	set of available transmitter types for each optical band in B, in increasing required FSU order	f_a	final set of FSUs assigned to demand d
r	transmitter type (macroscopic parameters)	w_a	final transmitter power for demand d
r_d	Maximum reach of a transmitter type r	S_t	total simulation time
r_f	number of consecutive FSUs consumed per transmitter type r	t	current simulation time
d	One particular traffic demand (source-destination)	d_{rt}	boolean, TRUE if demand d is routed, FALSE otherwise

formalism which we develop here accounts for this restriction, as it is detailed in Section 4.2, so the impact of SRS on FWM can, indeed, be considered as a secondary effect.

3. A planning Tool for Optical Multi-Band Networks

Our objective is to assess the potential of OMB systems to upgrade BT's 21CN network and whether OMB is a future-proof and viable alternative to legacy, C-band-only, systems. To do so, we have developed a planning tool that is based on a multi-band routing engine. The latter exploits a novel MB-PLA-RMSA algorithm which ensures that routing: i) is implemented with an efficient spectrum and modulation-format assignment; and ii) takes into account the physical layer performance of the selected optical paths via the formalism of eqs. (1)–(5). In this way, the planning tool ascertains the conditions that maximize the total capacity of the network while it minimizes the request blocking probability. To develop this algorithm, we have extended our previous routing algorithms in C-band systems [29]–[40] to readily introduce and activate at will any of the optical bands in Figs. 2 and 3.

The MB-PLA-RMSA algorithm completes the operation in three stages, as follows. *First stage:* the network topology is defined including the connectivity pattern between the nodes and the traffic matrix is set. Moreover, the *k-shortest paths* for all the network node pairs are derived. With the aid of the parameters listed in Table 1, the operations during the first stage are detailed below:

INPUT: Network topology including nodes, edges and amplifiers $G(N, E, A)$. Define the optical bands B *engaged*. Definition of the capacity C_B per band. Definition of traffic matrix T. Average time duration D_t of the demands and average inter-arrival time D_i between two consecutive demands. Definition of the available line-rates LR and their distribution on the demands.
Network Topology Implementation:
1: **for all** $n_i \in N$ **do**
2: **for all** $n_j \in N$ **do**
3: Compute k shortest-paths using the Yen's algorithm and store the results to $K(n_i,n_j)$
4: **end for**
5: **end for**
6: t=0
7: **while** t< S_t
8: Generate a new demand d; Add d to D;
9: **end while**

Second stage: a preliminary Spectral and Modulation Assignment (SMA) is made and the physical layer performance assessment is carried out with the aid of eqs. (1)–(5). In particular, in the first step of the second stage, a preliminary spectrum and modulation format assignment (SMA) is made. As only end-to-end transparent paths are considered in this work, a lightpath is

blocked only if no continuous spectral slots are available across the designated bands to support the end-to-end connection. These operations are illustrated below:

Spectral and Modulation Assignment (SMA) and PL entanglement:

10: **while** D is not empty **do**
11: Consider the first demand $d \in D$;
12: B_d=B; K_d=k-shortest paths from d_s to d_n in $K(n_i,n_j)$; d_{rt}=false;
13: **while** B_d is not empty AND d_{rt}=false **do**
14: Consider the first band $b \in B_d$;
15: **while** K_d is not empty AND d_{rt}=false **do**
16: Consider the first path $p_c \in K_d$;
17: Calculate the set of r $\in R_B$ denoted as R_d assuming band b and line-rate d_{lr};
18: **for all** $r \in R_d$ **do**
19: **if** ($r_d < p_c$ *distance*)
20: Remove r from R_d;
21: **end if**
22: **end for**
23: **while** R_d is not empty AND d_{rt}=false **do**
24: Consider the first $r_c \in R_d$ assuming band b *and* line-rate d_{lr};
25 : **while** $FSU_i < C_b$ AND d_{rt}=false **do**
26: Calculate the next available set of FSUs FSU_n in the path p_c starting from FSU_i using the First Fit (FF) route algorithm
27: **if** (route found in FF)

In the second step of the second stage, the OSNIR to the assigned lightpaths is estimated taking into account the physical layer effects described via Eq. (2)–(5) (this is designated in line 28 of the pseudo-code as "Execute PLC using Path OSNIR").

Physical Layer Performance:

28: Execute Physical Layer Check (PLC) using *Path OSNIR*
29: **if** PLC == true
30: Assign the demand using *Path Allocation (d,b,pc,d_{bw});*
31: **end if**
32: **end if**
33: **end while;** Remove r_c from R_d;
34: **end while;** Remove p_c from K_d;
35: **end while;** Remove b from B_d;
36: **end while**
37: **if** (d_{rt}=false)
38: Block demand d;
39: **end if**
40: **end while**

Third stage: the final assessment on network's throughput is completed. During this step, the engine estimates: a) the likehood OSNIR for the candidate lightpath due to the presence of the already accepted lightpaths; b) the potential degradation this new lightpath may incur to the OSNIR value of the already allocated lightpaths. If the corresponding OSNIR values from these two estimations are higher than the threshold set for a targeted BER, then this lightpath is admitted, otherwise it is rejected. In this case, the rejected lightpath is re-iterated using the next available path from the sorted k-shortest paths based on the network-wide operation policies set on the routing engine. A lightpath is successfully established if contiguous spectral slots are available over the end-to-end transparent path with acceptable physical layer performance; else the candidate lightpath is blocked. Then the network is populated with lightpaths as it is described below:

Path Allocation:

41: Allocate path p_a= p_c in the network;
42: Allocate set of frequency slot units f_a=f_c in the optical band b across the path p_a in the network;
43: Allocate transmitter r_a=r_c across the path p_a in the network;
44: *Set* w_a as the power of transmitter r_a;
OUTPUT: Utilisation of frequency slot units, finalisation of modulation format for a given line-rate, the consumed optical band and the power channel for all demands in the set D.

The corresponding flowchart to complete the tasks of this multi-band routing engine is shown in Fig. 4.

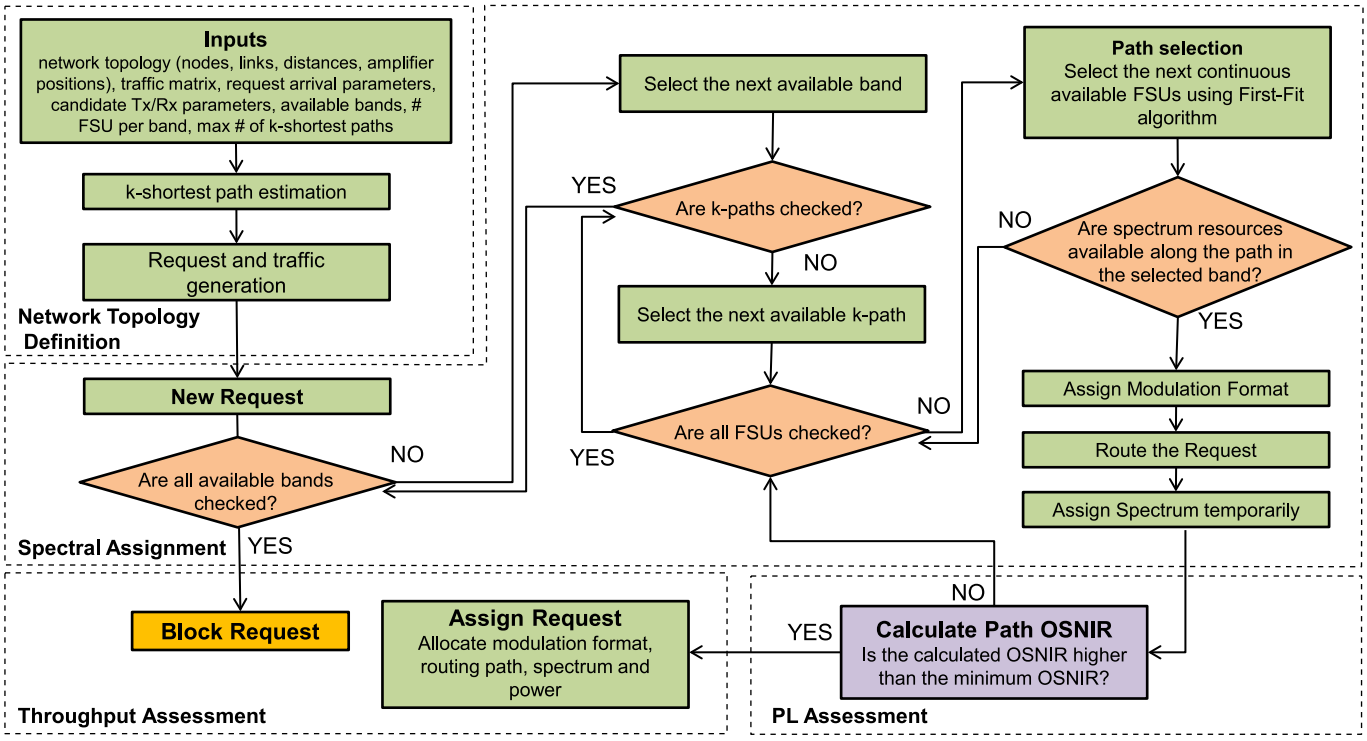

Fig. 4. The flow chart of the multi-band routing engine.

TABLE 2
Details of the Amplification (Sub)-Bands Used in Our Study

	Spectrum (nm)	*Range (nm)*	*Number of FSUs*	*a (dB/km) @ central λ*	*D (ps/nm/km) @ central λ*
O-band	1290-1315	25	350	0.37	0
S_1-band	1455-1480	25	275	0.246	12.05
S_2-band	1485-1510	25	265	0.23	14
C-band	1530-1565	35	350	0.211	16.9
L-band	1570-1615	45	425	0.209	19.4

4. System Configuration and Approximations

As it is evident from Fig. 2, the ITU standardization decisions led to optical bands of dissimilar spectral width across the SMF's second and third low-attenuation window. To minimise the complications in system design due to this uneven bandwidth partitioning, we have further sub-divided the entire spectrum in sub-bands as shown in Table 2. The corresponding fiber attenuation and local dispersion parameters for the central wavelength of each sub-band are also shown in the last columns of Table 2.

In particular, the S-band is split into two sub-bands since a single TDFA may not provide sufficient power per channel (e.g. more than -2 dBm) at its output for the entire group of channels within the full S-band. Moreover, the spectral width of the different DFA gain profiles is not an exact match to the nominal spectral width of the corresponding bands. For example, the gain bandwidth of a TDFA is extended to >5 nm in the E-band spectrum which means that the existing band classification has a degree of arbitrariness. For the same reason, although we have assumed a 5 nm guard band between optical bands, at the end a spectrum of $\sim$20 nm was left unused between the S_2 and the C-band due to the mismatch between the amplification bandwidth of a TDFA and the nominal

TABLE 3
Details of the Transportation Granularities Per Flow

	Modulation Format	*Channel Bandwidth (GHz)*	*Channel spacing (GHz)*	*Data Rate (Gb/s)*	*Req. OSNIR (dB) (BER=10^{-3})*
100G (Dense)	PM-QPSK	28	37.5	100	9.8
100G (Coarse)	PM-QPSK	28	75/112.5	100	9.8
200G (Coarse)	PM-16QAM	28	75/112.5	200	16.55
200G (16-QAM)	PM-16QAM	28	37.5	200	16.55
400G (32-QAM)	PM-32QAM	45	50	400	19.5

spectral extend of the S-band. Consequently, a different partitioning of the S-band and/or guard band selection would allow the existance of a third sub-band (the S_3; not considered here).

Finally, as the FSU width is defined in the frequency domain while the optical bands are defined in the wavelength domain, additional discrepancies arise. For example, we have assumed FSUs spaced by 12.5 GHz so even though the O, S_1 and S_2 are extended over 25 nm of spectrum, the number of FSUs within each band is different.

For a system design and modeling that it is self-consistent across all optical bands, we have introduced a number of approximations as follows:

a) For the bands of Table 2, the amplifier gain exactly compensates the total losses of the preceding SMF span. This figure includes accounts for the fibre loss and the loss due to the two band-filters of Fig. 3(a) which are of the order of 2 dB.

b) It is assumed that every optically transparent node across an end-to-end path employs a WSS in its transit path. In this way, all channels in a given band are entering the fibre of the next link at the same nominal power level. This power equals to the value of the mostly attenuated channel in the different input fibre. In this way, P_{ch} can remain constant across an end-to-end path, albeit this decision may, somewhat, degrade the OSNR performance of longer paths. Under this assumption, Eq. (1) is reduced to

$$OSNIR = \frac{P_{ch}}{P_{ASE} + P_{FWM}} \tag{6}$$

c) As detailed in [41]–[42], Eq. (2)-(4) strictly apply only for transmission paths with equidistant optical amplifiers, which is not the case in BT's 21CN network. Therefore, although we consider the real inter-node distances, as of Fig. 1, for the calculation of FWM in Eq. (2)-(4) we have assumed equidistant amplifier spacing in all links. In particular, the distance, $L_{amp,av|link}$, equals to the length of a given link divided by the real number of amplifiers in it. This approximation allows to calculate $P_{FWM,intra}$ using Eq. (3) in a straightforward way. Moreover, to calculate $P_{FWM,inter}$ using Eq. (4), first we calculate the $P_{FWM,inter|link}$ for a given link and then the FWM of an end-to-end path, $P_{FWM,inter}$, is estimated by adding the contributions from all links.

d) An O-band multi-channel unrepeated transmission with amplified links is facing it's own challenges which are beyond the scope of this work. As such, the O-band in this work is employed only in the context of un-amplified point-to-point links to serve short-range connections (28.5% of the links in BT's network are short-range i.e., $<$70 km). To account for this effect, the optical bands are engaged in the MB-RMSA algorithm in the following sequence: we always start from the O-band followed by the C-band, the L-band and finally the S-band.

4.1 Transportation Parameters and Operational Margins

In this work, we consider widely accepted transportation granularities like 100G, 200G and 400G per channel with system-level specifications as in Table 3. All system parameters listed in Table 3 have a direct impact to the attainable network capacity. For example, wavelength blocking depends

on the attainable physical layer performance as well as the available number of channels. Therefore, parameters like "channel optical bandwidth" and "channel spacing" have a direct impact on the attainable blocking. Because of this, we made an effort to consider as many common values for these parameters as possible to allow meaningful comparisons between different configurations and to avoid a possible trade-off between the requested capacity and attainable connectivity.

The ability of a particular technology to reach a higher transportation capacity critically depends on the optimal value of the channel power P_{ch}. In turn, it is this value that defines the operational point of a system i.e. whether a channel or all channels are operated in the ASE-limited or the fibre nonlinearities-limited regime. As the value of P_{ch} may not remain constant over time, we quantify in our analysis the impact of *operational margins* to the ability of a system to reach a higher transportation capacity. We introduce the operational margins in our analysis using two different methods: the first is to directly consider the OSNIR degradation in Eq. (6) due to power depletion, as detailed in [43], that decreases P_{ch}. This power degradation is attributed to a number of physical layer effects like: a drop in the output power of the transmitters due to aging; the excessive losses of optical components; imperfect channel equalisation etc. The collective outcome of these processes is designated as a *power-margin* in the remaining part of this work. The second method is to ignore the actual physical layer effects and to set a higher OSNIR threshold value for a channel to be admissible. This higher threshold corresponds to lower BER values compared to Table 3 e.g. BER$\sim 10^{-5}$. This approach is identified as *higher-BER margin* in this work.

4.2 A Rigorous Estimation of the Optimal Launch Power P_{ch}

In an OMB transmission system, the optimal launch power (P_{ch}) is a function of the characteristics of each band, like the fibre attenuation $\alpha(\lambda)$ and dispersion $D(\lambda)$. In turn, the value of P_{ch} impact the strength of fibre nonlinearities that lead to intra-band and inter-band power exchanges. To account for these effects, a rigorous mathematic optimization procedure has been applied using as a merit function the OSNIR. We define the quantity $A(P_{S_1}, P_{S_2}, P_C, P_L)$:

$$A\left(P_{S_1}, P_{S_2}, P_C, P_L\right) = \sum_b \left(\frac{1}{OSNIR_b\left(P_{S_1}, P_{S_2}, P_C, P_L\right)} \right)^2 \tag{7}$$

where $P_{S_1}, P_{S_2}, P_C, P_L$ represent the power channel that is spectrally located in the middle of S_1, S_2, C and L-bands at the beginning of each link, respectively. The parameter b stands for the band index, which in our work here takes the values 1 to 4, corresponding to the OSNIR of the bands S_1, S_2, C and L.

The optimization problem is formally stated as the requests to find the values of $P_{S_1}, P_{S_2}, P_C, P_L$ that minimize the function $A(P_{S_1}, P_{S_2}, P_C, P_L)$. In order to deduce meaningful and self-consistent results in the minimization of $A(P_{S_1}, P_{S_2}, P_C, P_L)$, a number of conditions need to apply:

i) The OSNIR value (eq. 1–6) depends on the path length and the distribution of channels, at a given moment, in the links within a given path. Here, we are considering the worst possible scenario which consists of the longest path in the network of Fig. 1 under the condition of fully loaded optical bands with channels.

ii) The condition $P_{S_1}, P_{S_2}, P_C, P_L \leq P_{\max}$ is introduced to set an upper value to P_{ch} in a particular band as gain saturation effects limit the maximum output power a given DFA may provide. For links with fully loaded bands and the parameters listed in Table 2 and 3, a typical value is $P_{\max} < +1$ dBm.

iii) A further constraint $P_{tot,SRS} \leq +21\ dBm$ is also set to ensure that the impact of SRS on FWM is a secondary effect, according to Fig. 4(b) of [9].

Under these constraints, the optimization returns the values $P_{S_1}, P_{S_2}, P_C, P_L$ that lead to a balanced OSNIR performance across all bands. Moreover, the performance is optimised for the most prone to blocking paths. The derived optimal P_{ch} values under the conditions (i)-(iii) are shown in Table 4. It is pointed out that this optimization method can also be applied recursively to estimate the optimal power levels of the other channels within a particular band. Moreover, the introduction

TABLE 4
Optimal Channel Powers for Different System Configurations

	Multi-band			*C-band*	
	Dense (37.5 GHz)	*Coarse* (75 GHz)	*Coarse* (112.5 GHz)		
P_C (dBm)	-8.3	-5.3	-4.0	P_{100G}	-2.2 (dBm)
$OSNIR_C$ (dB)	*17.8*	*18.5*	*18.8*		
P_L (dBm)	-9.0	-6.0	-4.6	P_{200G}	-2.2 (dBm)
$OSNIR_L$ (dB)	*17.2*	*18.3*	*18.7*		
P_{S1} (dBm)	-0.2	-0.4	-0.5	P_{400G}	-1.0 (dBm)
$OSNIR_{S1}$ (dB)	*14.6*	*15.4*	*15.8*		
P_{S2} (dBm)	-1.4	-1.0	-1.0		
$OSNIR_{S2}$ (dB)	*16.6*	*16.7*	*16.9*		

of appropriate weights in Eq. (7) would allow to give emphasis to the performance of a particular band at the expense of the performance of other bands. Finally, it is pointed out that the use of closed-form formulae like those in Eq. (1)–(6) simplifies to the greater extend this optimization process.

4.3 Metrics Used to Assess the Network-Wide Performance

To benchmark the alternative network capacity upgrade scenarios in a consistent way, we introduce the quantity *Cumulative Traffic Blocking (CTB)* which is defined by

$$CTB = \frac{\text{total blocked traffic(Tb/s)}}{\text{total offered traffic (Tb/s)}} \tag{8}$$

CTB depends on the topology of the entire network and the interconnection pattern between the nodes. For a given network, *CTB* provides a quantitative measure of the requests/traffic volume that has been rejected, at a network-wide scale, either due to frequency slot unavailability or due to physical layer effects.

Another important performance analysis consideration is whether it is a necessity to roll-out multi-band systems across all links in a network at once or this may be done gradually. For the latter, we introduce the quantity "*band utilisation*" which is defined as the ratio between the number of frequency slots used for transportation over the total number of frequency slots in this band (as designated in Table 2).

5. Results and Discussion

As it has already pointed out, in this work we are aiming to assess the potential of optical multi-band systems to upgrade BT's backbone network against legacy alternatives. To do so, we employ the planning tool detailed in Section 3 under the methodology and the specifications presented in Section 4. This task is completed in a number of steps:

a) The network topology of Fig. 1 is introduced that sets the number of nodes, the intra-node distances and the connectivity pattern between those nodes.
b) Then, we steadily increase the traffic across the network; a uniform traffic demand is assumed in all connections between any node pairs in all cases. The corresponding traffic flows are generated by means of a pseudo-random sequence.
c) To gratify the continuously increasing demand for higher capacity, two alternative approaches are considered: i) a single-fibre system exploiting an OMB WDM (OMB-WDM) transmission in S, C and L bands; ii) a Space Division Multiplexing (SDM) system that employes (legacy) WDM in the C-band only. In the SDM case, a higher network capacity is reached by increasing the line-rate of channels e.g. from 100G to 200G and then to 400G and then by lighting-up additional legacy fibres. The number of active fibres in the SDM example is designated, hereafter, as *fibre cardinality (FC).*

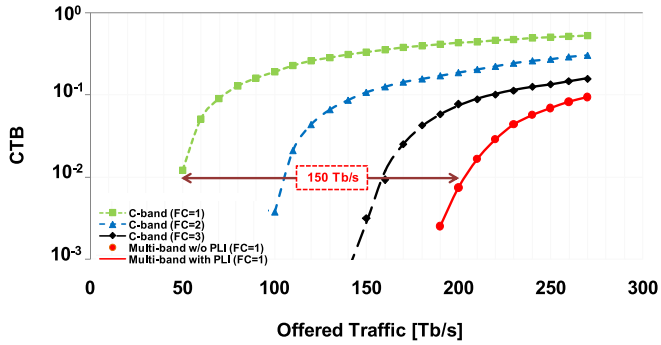

Fig. 5. *CTB* vs offered traffic for legacy and OMB systems with 100G transportation granularity. CTB degradation is only due to spectral slot exhaustion.

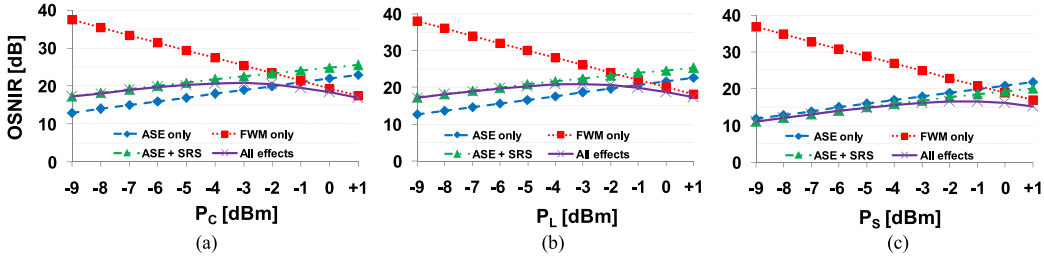

Fig. 6. The OSNIR v. Pch evolution in the reference scenario for (a) C-band, (b) L-band and (c) S-band of an OMB system one of the longest paths in BT's network.

d) In the next step, the channels are routed under the WRNs mode by means of the routing engine and the MB-PLA-RMSA algorithm that is presented in Section 3. As detailed in Section 3, only end-to-end transparent paths are considered i.e. no regeneration at an intermediate/transit node is performed. The Yen's algorithm [44] is used to derive up to $k = 10$ shortest paths between any pair of nodes in all cases.
e) As the number of channels are increasing, the CTB of eq. (8) is increasing due to spectral slot unavailability and/or due to physical layer effects.

To establish what we identify as the *reference scenario*, we assume that all flows in BT's network are transported by means of 100G channels with the 'Dense' specifications in Table 3. The threshold for admitting a lightpath was set for a BER $\sim 10^{-3}$ which corresponds to an OSNIR value of 9.8 dB. In Fig. 5, we observe that for a *CTB* of 1%, legacy SDM systems with more than three fibres ($FC = 3$) are required to match the capacity of a multi-band system with $FC = 1$. In particular, this multi-band system may transport 150 Tb/s, 100 Tb/s and 45 Tb/s higher capacity than a legacy system with fibre cardinality $FC = 1, 2$ *or* 3, respectively. In this reference scenario, physical layer effects have a marginal contribution to CTB degradation in either systems. Therefore, the CTB worsening is exclusively due to spectral slot exhaustion.

It is of interest to further probe on the impact the different physical layer effects of Section 2.3 have to the performance of the most vulnerable path in BT's network which is of 1050 km in length and the path is fully loaded with channels. In Fig. 6(a), (b) and (c), the OSNIR v. channel power (P_{ch}) is shown for the C, L and S-bands, respectively. To get this result, the OSNIR is iterated against the P_{ch} value at the particular band of interest while the corresponding P_{ch} for all channels in the other bands gets the fixed value of Table 4.

It is observed that for the C and L-bands, the OSNIR is always higher than the required 9.8 dB. Moreover, it is evident that for the optimal power level of -8.3 dBm (see Table 4), the two bands operate at the OSNR-limited regime; for these bands fibre nonlinearities become important for power levels > -2 dBm. On the other hand, the S-band system is more susceptible to the impact

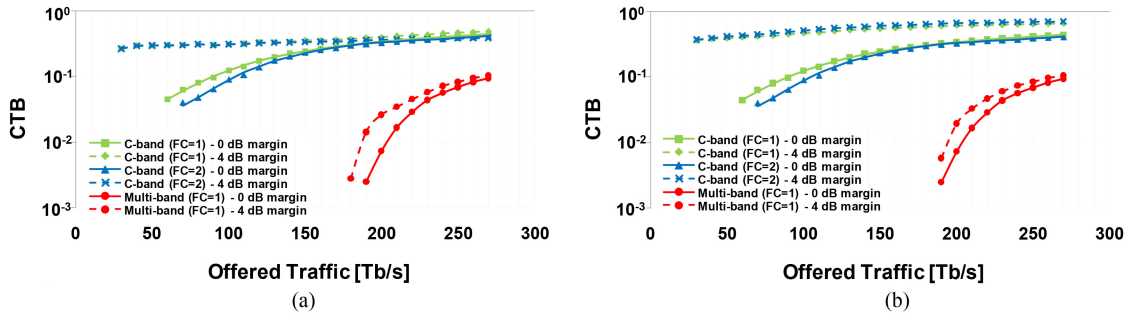

Fig. 7. *CTB* vs offered traffic for legacy and OMB systems with a 100/200/400G transportation granularities for legacy systems and 100G for OMB systems: (a) the power-margin estimation method was used, (b) the higher-BER estimation method was used.

of fibre nonlinearities and in particular SRS. Specifically, for the optimal power level $P_{ch} = -1.4$ dBm (see Table 4) the main transmission impairment for the S-band is SRS. The SRS impacts the OSNIR performance at a considerably lower P_{ch} value compared to what FWM does.

The next step in our study is to consider the capacity upgrade of legacy systems via operating the corresponding channels at higher line-rates. Therefore, legacy, C-band, line-rates scale to a mix of 100G, 200G and 400G -with equiprobable statistics- using the system parameters detailed in Table 3. In contrast the line-rate of OBM systems remains at 100G per flow as it in the reference scenario. The corresponding *CTB* v. traffic for this scenario is shown in Fig. 7(a).

Apparently, the legacy system has a significantly higher blocking compared to an OMB system mainly due to the very high OSNIR requirements of the 200G and 400G line-rates. As the 400G flows use a 32-QAM modulation format, they require almost 10-dB higher OSNIR to attain the same BER with a 100G channel system. Consequently, for this scenario there will be considerable network blocking even under a light traffic load. A physical layer analysis similar to the one shown in Fig. 6 was carried out for this configuration too, revealing that the main degradations for a legacy system is due to ASE noise and FWM.

Given this marginal performance of legacy systems at higher line-rates, we wish to investigate the impact of the operational margins to their viability. As it is shown in Fig. 7(a), the introduction of an operational margin, based on the power-margin estimation method (see Section 4.1), severely limits the attainable throughput of legacy systems that manifest an unacceptable blocking. Under this operational margin, the systems are employed at a P_{ch} of 4 dB lower than their optimal value which means they are deeply in the ASE-limited regime. As a result, both 200G and 400G channels fail short to the required OSNIR even for medium-length paths so this capacity upgrade alternative is very restrictive for a legacy system. On the contrary, performance degradation for the OMB systems due to the physical layer effects is marginal.

In Fig. 7(b) the operational margins have been re-iterated by means of the alternative method which is based on a higher-OSNIR threshold (see Section 4.1). As before, the introduction of a 4 dB margin renders legacy SDM systems equally inoperable. On the other hand, the impact of operational margins onto an OMB system is less severe. The physical layer analysis of an OMB system revealed that SRS and ASE noise are the most detrimental effects in the S-band. The higher impact of ASE is due to to the higher attenuation in this band (and hence the need for higher gain in the corresponding TDFA).

A comparison between Fig. 7(a) and Fig. 7(b) shows that OMB systems are slightly more sensitive to margin analysis when is estimated via the power-margin method.

To further probe into these results for OMB systems, we investigated the impact of a sparsely-populated WDM channel scheme where optical bandwidth is traded for lower fibre nonlinearities. To do so, we considered systems with 75 GHz (6 spectral slots) and then 112.5 GHz (9 spectral slots) channel spacing. When systems with wider channel spacing are employed, the impact of FWM and SRS is expected to decrease.

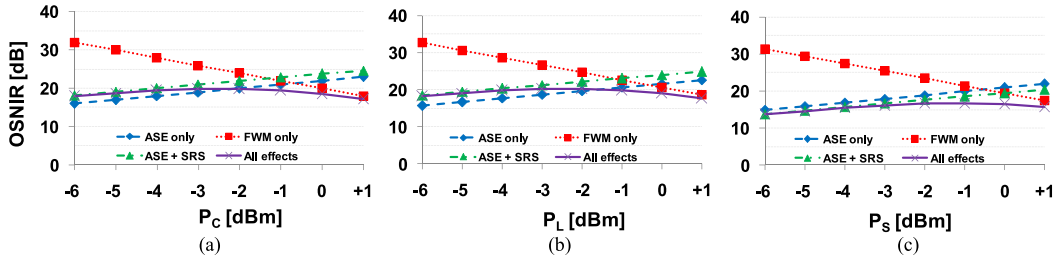

Fig. 8. The OSNIR v. Pch evolution for a 75 GHz channel spacing system (a) C-band, (b) L-band and (c) S-band in the OMB system.

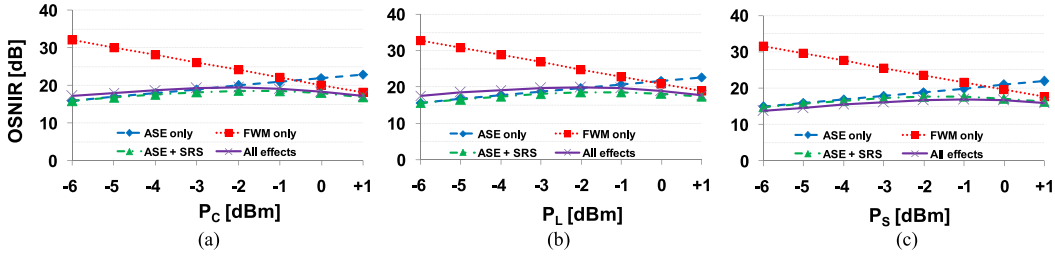

Fig. 9. The OSNIR v. Pch evolution for a 112.5 GHz channel spacing system (a) C-band, (b) L-band and (c) S-band in the OMB system.

The OSNIR v. channel power evolution for a 75 GHz channel spacing is shown in Fig. 8(a), (b) and (c) for the C, L and S-bands, respectively. From Fig. 8 it is observed that C and L bands are mainly ASE-limited while the S-band is SRS limited. The derived optimal P_{ch} values are slightly higher than the values of Table 4 which in turn, led to about 0.16 dB higher OSNIR for the channels in the S-band; 0.75 dB higher for the channels in the C-band and 1 dB higher for the L-band. When the channel spacing is increased to 112.5 GHz (Fig. 9), the corresponding OSNIR values increase by 0.3 dB for the channels in the S-band, 1 dB for the channels in the C-band and about 1.5 dB for L-band (see Table 4).

Our analysis reveals that as channel spacing increases, the strength of fibre nonlinearities is decreasing but not at a rate that would substantially impact the overall system performance. This is because the optimization of Section 4.2 returns P_{ch} values that prohibit the system to enter into the deep non-linear regime. Moreover, as the number of channels becomes half and one-third to the original configuration with a channel spacing of 75 GHz and 112.5 GHz, respectively, an improvement in physical layer performance may not necessarily lead to a higher transported capacity due to the subsequent smaller number of available channels.

However, the OMB transmission under the sparsely-populated WDM channel scheme may offer significantly enhanced flexibility. For example, as the S-band is more susceptible to physical layer effects, we illustrate the following operational scheme: the S-band is used for the transportation of 100G channels only while C and L bands are reserved to transport 200G channels only in conjunction with a 75 GHz channel spacing (see Table 3). This configuration is benchmarked against a legacy SDM system that employs 100/200/400G under the 'dense' set-up in Table 3 (as in Fig. 7). In this case, the optimal values of P_{ch} were re-derived via Eq. (7) with the additional constraints for OSNIR $>$17 dB to account for the higher line-rates in C and L bands. Through this process the performance of C and L bands is boosted at the expense of S-band, which is although slightly degraded from SRS, the attainable OSNIR is safely above the 9.8 dB threshold for 100G channels (see Table 5). As it is shown Fig. 10, although OMB and legacy systems are equally hit by physical layer effects at higher line-rates, an operator may explore the flexibility these systems are offering either to reduce the impact of these effects or to pursue a less aggressive policy for capacity increase by means of higher line-rate channels.

TABLE 5
Power Per Channel and Attainable OSNIR for the Flexible Channel Scheme

	P_{ch} (dBm)	OSNIR (dB)
S_1-band	-0.1	14.1
S_2-band	-0.7	14.6
C-band	-2.0	19.1
L-band	-2.0	20.6

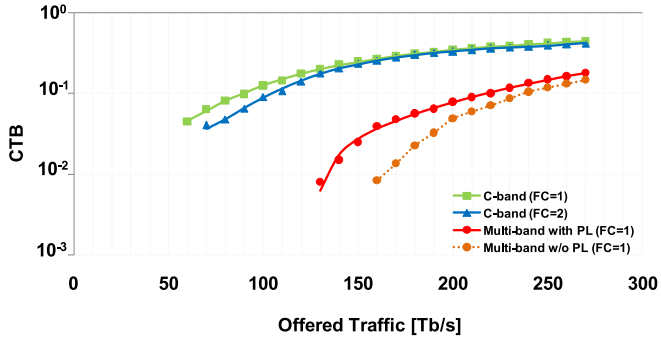

Fig. 10. Comparison of a dense C-band (as in Fig. 7) vs a flexible channel packing in MB with 100G in the S-band and 200G in C and L bands.

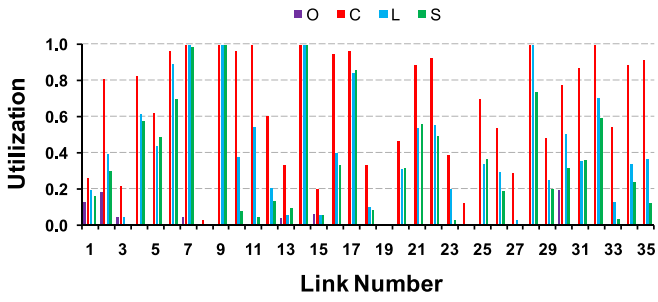

Fig. 11. Link *utilisation* in BT's 21CN network for a 203 Tb/s transportation capacity ($CTB = 1\%$).

Finally, we are considering a roadmap for the roll-out of multi-band transmission systems. Inevitably any conclusion is inextricably associated to link utilisation performance each band is demonstrating. For this particular study, we consider the reference scenario and we set $CTB = 1\%$ as the threshold value which, after Fig. 5, corresponds to 203 Tb/s throughput. At this capacity, the per-band utilisation for the links of Fig. 1, is shown in Fig. 11.

One may observe that some links are heavily utilised while others are considerably underutilised. In particular, links #7, #9, #14, which are of a short/medium distance and they are centrally located in BT's network topology, feature the highest utilisation. In contrast, links #8, #19, #24, which are of a longer length and they are located in the BT network periphery, are poorly utilised mainly due to physical layer limitations.

Nevertheless, as Fig. 11 shows only a snapshot of band utilisation for this particular capacity, we have re-iterated the utilisation of these links for different network capacities. Therefore, Fig. 12 shows the *utilisation* of the optical bands for different transportation capacities. In this particular example, approximately half of these links need to engage the L-band to achieve a 50 Tb/s capacity while the S_1 is not engaged until a capacity of more than 100 Tb/s is required. Evidently, not all links need to carry all bands simultaneously to upgrade this network. Instead, the operator may deploy them on-as-needed basis to certain links according to the increase in the requested capacity.

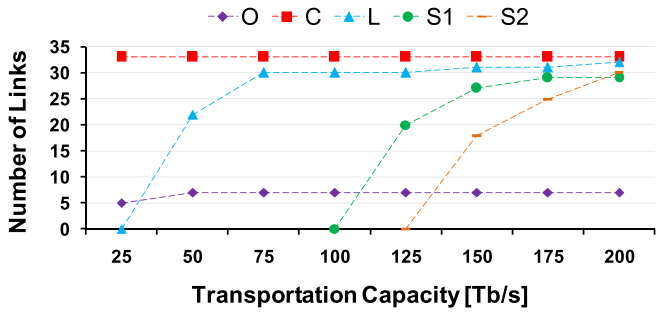

Fig. 12. Number of links employing each band for different transportation capacities in BT's 21CN network.

5.1 Discussion

The previous analysis reveals that multi-band systems could be a viable option to upgrade a national-scale network without trading connectivity for higher capacity. This technology is of particular interest in network segments suffering from fibre exhaustion. Moreover, it offers significant engineering flexibility with respect to the adopted line-rates across the network. Our analysis reveals that the roll out of OMB systems could be carried out in phases to reduce first-day capital expenditure. Nevertheless, the full potential of multi-band systems is not yet fully evident as considerable research efforts are still needed at system and technology level. Particular attention should be paid to the O and E bands and specifically to the advances in system design needed for these systems to be fully integrated with the more mature S, C and L bands.

6. Conclusion

In this work we detail the potential of a multi-band system that employs the S, C and L bands as well as the O-band in un-amplified links, to upgrade BT's 21CN network. Our studies were based on a planning tool that exploits a novel RMSA engine that takes into account the main physical layer degradation phenomena in a spectrally extended transmission window, like ASE, FWM and SRS, by means of closed-form formulas. The sufficiently low complexity of the latter allowed us to carry out power optimizations at a reasonable time scale. We have shown that under such operational conditions, optical multi-band systems may outperform legacy C-band only systems in terms of the attainable transported capacity. Finally, we have shown that the roll out of these multi-band systems could be planned in phases in order to limit first-day capital expenditure. Nevertheless, these results have also indicated the need to intensify research efforts to fully utilize the potential of optical multiband transmission.

References

[1] A. Lord, A. Soppera, and A. Jacquet, "The impact of capacity growth in national telecommunications networks," *Philosoph. Trans. Roy. Soc. A*, vol. 374, 2016, Art. no. 20140431.
[2] A. Stavdas, "Architectural solutions towards a 1,000 channel ultra wideband WDM network," *Opt. Netw. Mag.*, vol. 2, no. 1, pp. 51–60, 2001.
[3] P. Bayvel *et al.*, "Maximizing the optical network capacity," *Philos. Trans. R. Soc. A Math. Phys. Eng. Sci.*, vol. 374, no. 2062, Mar. 2016.
[4] A. Stavdas, "Ensuring end-to-end QoS in an integrated access-core based on massive WDM," *Access Netw. In-house Commun.*, *OSA Opt. Photon. Congr.*, 2010.
[5] A. Stavdas, M. Manousakis, C. Scahill, and A. Hadjifotiou, "The design of a free-space multi/demultiplexers for ultra-wideband WDM networks," *IEEE J. Lightw. Technol.*, vol. 19, no. 11, pp. 1777–1784, Nov. 2001.
[6] A. Stavdas, "A single WDM Multi/Demultiplexer for all SMF transmission windows in 1280–1680 nm," *IEEE Photon. Technol. Lett.* vol. 14, no. 10, pp. 1542–1544, Nov. 2002.
[7] M. Cantono *et al.*, "On the interplay of nonlinear interference generation with stimulated Raman scattering for QoT estimation," *J. Lightw. Technol.*, vol. 36, no. 15, pp. 3131–3141, 2018.

[8] F. Hamaoka *et al.*, "Ultra-wideband WDM transmission in S-, C-, and L-bands using signal power optimization scheme," *J. Lightw. Technol.*, vol. 37, no. 8, pp. 1764–1771, 2019.
[9] D. Semrau, R. I. Killey, and P. Bayvel, "The Gaussian noise model in the presence of inter-channel stimulated Raman scattering," *J. Lightw. Technol.*, vol. 36, no. 14, pp. 3046–3055, 2018.
[10] D. Semrau, R. I. Killey, and P. Bayvel, "A closed-form approximation of the Gaussian noise model in the presence of inter-channel stimulated Raman scattering," *J. Lightw. Technol.*, vol. 37, no. 9, pp. 1924–1936, 2019.
[11] A. Ferrari *et al.*, "Assessment on the achievable throughput of multi-band ITU-T G. 652. D fiber transmission systems," *J. Lightw. Technol.*, vol. 38, no. 16, pp. 4279–4291, 2020.
[12] J. Renaudier, "100nm ultra-wideband optical fiber transmission systems using semiconductor optical amplifiers," in *Proc. Eur. Conf. Opt. Commun.*, 2018, pp. 1–3.
[13] M. Morimoto, H. Ogoshi, J. Yoshida, S. Takasaka, A. Sano, and Y. Miyamoto, "Co-propagating dual-order distributed Raman amplifier utilizing incoherent pumping," *IEEE Photon. Technol. Lett.*, vol. 29, no. 7, pp. 567–570, Apr. 2017.
[14] J. W. Dawson *et al.*, "E-band Nd^{3+} amplifier based on wavelength selection in an all-solid micro-structured fibre," *Opt. Exp.*, vol. 25, no. 6, Mar. 2017, Art. no. 6524.
[15] "Commercially available amplifiers," [Online]. Available: https://www.fiberlabs.com
[16] M. Karasek and M. Menif, "Serial topology of wide-band erbium-doped fibre amplifier for WDM applications," *IEEE Photon. Technol. Lett.*, vol. 13, no. 9, pp. 939–941, Sep. 2001.
[17] Q. Jiang, X. Liu, Q. Wang, and X. Feng, "Dynamical gain control in the serial structure C+L wide-band EDFA," *IEEE Photon. Technol. Lett.*, vol. 16, no. 1, pp. 87–89, Jan. 2004.
[18] T. Sakamoto, A. Mori, M. Shimizu, and I. Introduction, "Rare-earth-doped fibre amplifier for eight-channel CWDM transmission systems," in *Proc. Opt. Fiber Commun. Conf.*, 2004.
[19] T. Sakamoto, M. Y Shin-ichi Aozasa, and M. Shimizu, "Hybrid fibre amplifiers consisting of cascaded TDFA and EDFA for WDM signals," *J. Light. Technol.*, vol. 24, no. 6, pp. 2287–2295, Jun. 2006.
[20] B. A. Hamida *et al.*, "Wideband and flat-gain amplifier using high concentration Erbium doped fibres in series double-pass configuration," in *Proc. Int. Conf. Comput. Commun. Eng.*, 2012.
[21] A. Carena, G. Bosco, V. Curri, Y. Jiang, P. Poggiolini, and F. Forghieri, "EGN model of non-linear fibre propagation," *Opt. Exp.*, vol. 22, no. 13, Jun. 2014, Art. no. 16335.
[22] P. Poggiolini *et al.*, "A simple and effective closed-form GN model correction formula accounting for signal non-Gaussian distribution," *J. Light. Technol.*, vol. 33, no. 2, pp. 459–473, 2015.
[23] D. Uzunidis, C. Matrakidis, and A. Stavdas, "Closed-form FWM expressions accounting for the impact of modulation format," *Opt. Commun.*, vol. 440, pp. 132–138, 2019.
[24] D. N. Christodoulides and R. B. Jander, "Evolution of stimulated Raman crosstalk in wavelength division multiplexed systems," *IEEE Photon. Technol. Lett.*, vol. 8, no. 12, pp. 1722–1724, Dec. 1996.
[25] D. Semrau, R. Killey, and P. Bayvel, "Achievable rate degradation of ultra-wideband coherent fiber communication systems due to stimulated Raman scattering," *Opt. Exp.*, vol. 25, no. 12, 2017, Art. no. 13024.
[26] A. R. Chraplyvy, "Optical power limits in multi-channel wavelength-division-multiplexed systems due to stimulated Raman scattering," *Electron. Lett.*, vol. 20, no. 2, pp. 58–59, Jan. 1984.
[27] I. B. Djordjevic and A. Stavdas, "Analytical modeling of stimulated Raman scattering in WDM systems with dispersion compensated links," *J. Opt. Commun.*, vol. 24, no. 2, pp. 54–60, 2003.
[28] I. B. Djordjevic *et al.*, "Analytical modelling of fibre nonlinearities in amplified dispersion compensated WDM systems," *Int. J. Modelling Simul.* vol. 23, no. 4, pp. 226–233, 2003.
[29] C. Politi, V. Anagnostopoulos, C. Matrakidis, and A. Stavdas, "Physical layer impairment aware routing algorithms based on analytically calculated Q-factor," in *Proc. OFC*, 2006.
[30] V. Anagnostopoulos, C. Politi, C. Matrakidis, and A. Stavdas, "Physical layer impairment aware wavelength routing algorithms based on analytically calculated constraints," *Opt. Commun.*, vol. 270, no. 2, pp. 247–254, 2007.
[31] C. Politi, C. Matrakidis, and A. Stavdas, "Cross layer routing in transparent optical networks," in *Proc. IEEE/OSA OFC*, 2007.
[32] C. Politi *et al.*, "Integrated design and operation of a transparent optical network: A systematic approach to include physical layer awareness and cost function," *IEEE Commun. Mag.*, vol. 45, no. 2, pp. 40–47, Feb. 2007.
[33] V. Anagnostopoulos, C. Politi, C. Matrakidis, A. Stavdas, and A. C. Boucouvalas, "PLI-aware wavelength routing in optical networks," in *Proc. OFC*, 2009.
[34] C. Politi, V. Anagnostopoulos, and A. Stavdas, "Routing in meshed and clustered optical networks," in *Proc. ECOC*, 2010, pp. 1–3.
[35] C. Politi, V. Anagnostopoulos, and A. Stavdas, "PLI-aware routing in regenerated mesh topology optical networks," *J. Light. Technol.*, vol. 30. no. 12, pp. 1960–1970, 2012.
[36] C. Politi *et al.*, "Dynamic operation of flexi-grid OFDM-based networks," in *Proc. Opt. Fiber Commun. Conf.*, Mar. 2012.
[37] C. Politi, V. Anagnostopoulos, and A. Stavdas, "Cross-layer routing in clustered optical networks," *Photon. Netw. Commun.*, vol. 25, no. 1, pp. 1–9, 2013.
[38] E. Kosmatos, T. Orphanoudakis, C. Matrakidis, A. Stavdas, and A. Lord, "Switchless elastic rate node (SERANO) architecture: A universal node for optical grooming and adaptive networking," *IEEE/OSA J. Opt. Commun. Netw.*, vol. 8, no. 7, pp. A162–A170, Jul. 2016.
[39] C. Matrakidis, T. Orphanoudakis, A. Stavdas, and A. Lord, "Network optimization exploiting traffic grooming techniques under fixed and elastic spectrum allocation," in *Proc. Eur. Conf. Opt. Commun.*, 2014, pp. 1–3.
[40] Ć. Rožić, M. Savi, C. Matrakidis, D. Klonidis, and D. Siracusa, "A dynamic multi-layer resource allocation and optimization framework in application-centric networks," *J. Lightw. Technol.*, vol. 36, no. 20, pp. 4908–4914, 2018.
[41] D. Uzunidis, C. Matrakidis, and A. Stavdas, "Simplified model for nonlinear noise calculation in coherent optical OFDM systems," *Opt. Exp.*, vol. 22, no. 23, pp. 28316–28326, 2014.
[42] D. Uzunidis, C. Matrakidis, and A. Stavdas, "Application of a simplified FWM expression in mixed-fiber links," in *Proc. 24th Telecommun. Forum*, 2016, pp. 1–4.
[43] A. Stavdas, *Core and Metro Networks*. Hoboken, NJ, USA: Wiley, 2010.
[44] J Y. Yen, "Finding the k shortest loopless paths in a network," *Manage. Sci.*, vol. 17, no. 11, pp. 712–716, 1971.